Journal of Alloys and Compounds 696 (2017) 1059–1066

Contents lists available at ScienceDirect

Journal of Alloys and Compounds

journal homepage: http://www.elsevier.com/locate/jalcom

A study of shape memory alloy NiTi fiber/plate reinforced (SMAFR/SMAPR) Ti-Al laminated composites

Enhao Wang, Yao Tian, Zhenqiang Wang**, Feifei Jiao, Chunhuan Guo, Fengchun Jiang*

Key Laboratory of Superlight Materials & Surface Technology, Ministry of Education, Harbin Engineering University, Harbin, 150001, China

ARTICLE INFO

Article history:
Received 15 November 2016
Received in revised form
3 December 2016
Accepted 5 December 2016
Available online 7 December 2016

Keywords:
Shape memory alloy
NiTi fiber/plate-reinforcement
Tensile property
Compression property

ABSTRACT

In this work, shape memory alloy NiTi fiber reinforced (SMAFR) Ti-Al laminated composites containing ~41 vol%Ti and ~2.5 vol%NiTi was fabricated via vacuum hot pressing method. In order to accurately determine the reaction products of the fabrication process, a new kind of laminated composites i.e. shape memory alloy NiTi plate-reinforced (SMAPR) Ti-Al laminated composites was successfully prepared using the fabrication process that is similar to SMAFR laminated composites. Results showed that Al_3Ti and Al_3Ni are formed during fabrication process, and residual Al existed in the intermetallic layer. In addition, the quasi-static tensile test indicates that the tensile property of SMAFR laminated composites is superior to that of Ti/Al_3Ti composites. The fracture process of SMAFR laminated composite includes three basic stages: (I) delamination of interface of Ti/Al_3Ti; (II) fracture of Al_3Ti (and other products) and (III) fracture of NiTi fiber. Moreover, the novel SMAPR laminated composite possessed a good combination of high strength (compressive strength: 1105.4 MPa) and high plasticity (strain to failure: 5.1%), indicating that this kind of laminated composites is a new class of structural materials.

1. Introduction

Intermetallic titanium trialuminide (Al_3Ti) is a class of promising candidate for harsh environment due to its superior mechanical properties such as high strength, high modulus and low density [1–5]. Unfortunately, like most of intermetallics, Al_3Ti suffers from notoriously low ductility as the lack of slip systems and low mobility of dislocations during deformation at low temperatures [6]. In light of this, a class of metallic-intermetallic laminate (MIL) composites Ti/Al_3Ti was developed [7], which can be tailored to achieve a wide array of material properties and functionalities.

Originated from biomimetic motivation, MIL composites Ti/Al_3Ti have been fabricated and investigated thoroughly associated with their mechanical properties in the last several decades, including compressive, bending, and tensile properties, etc [8–11]. For example, Adharapurapu et al. [3] studied the fatigue crack propagation behavior of MIL composites using a single edge-notched bending and compact tension specimen. Their work demonstrated that the toughness and fatigue properties of MIL composites are improved greatly because of the bridging effect of ductile Ti, and the fracture toughness of the MIL composites Ti/Al_3Ti is almost identical to that of a common high strength structural steel. In addition, Jiang [12] and Zhou [13] conducted the interface tensile tests of the MIL composites Ti/Al_3Ti using Brazilian disc and direct tensile specimen, respectively, and investigated the failure mechanisms of the interface in MIL composites. Moreover, it is noticeable that the mechanisms of deformation and fracture of multi-layered composites can differ significantly from those of uniform materials. The presence of interfaces gives rise to deviation and deceleration of propagating cracks, which consequently increases the reliability of the material [3,14]. Several studies associated with the mechanisms of the formation of intermetallic Al_3Ti [15–17] in the MIL composites were reported, which provides evidence that Al_3Ti is preferentially formed at the temperatures below 1200 °C according to thermodynamics and reaction kinetics.

Recently, shape memory alloy (SMA) NiTi alloys received considerable attention due to its outstanding capabilities including recovering large deformations, generating high stress, and exhibiting high damping capacity [18–21]. Although NiTi binary alloys show excellent shape memory properties, they cannot be applied at temperatures above 100 °C owing to the low transformation temperatures (TTs). Therefore, ternary elements such as Hf, Zr, Pd, Pt and Au are added to NiTi to increase the TTs [22]. Moreover,

* Corresponding author.
** Corresponding author.
E-mail addresses: wangzhenqiang@hrbeu.edu.cn (Z. Wang), fengchunjiang@hrbeu.edu.cn (F. Jiang).

http://dx.doi.org/10.1016/j.jallcom.2016.12.062
0925-8388/

insufficient strength renders the application of SMAs extremely confined such that they are often introduced into other matrices to improve damping capacity [23], and accordingly they are used frequently in aerospace, mechanical engineering and civil engineering, etc [24–27]. In our previous work [28], a novel kind of shape memory alloy NiTi fiber-reinforced (SMAFR) laminated composites was synthesized, and the experimental results demonstrated that this composites has superior mechanical properties (compressive strength over 1200 MPa at room temperature) as well as damping capacity (damping factor over 0.04 from room temperature to 50 °C). The primary investigations into the microstructure of SMAFR laminated composites showed that some potential phases including Al_3Ti, Al_3Ni and $AlNi_2Ti$ form during the fabrication process. Unfortunately, due to the diffusion reaction among Ti, Al as well as NiTi, the microstructure of this kind of composites is of overwhelming complication. The uneven phases of the SMAFR laminated composites were formed and the fibers possibly overreacted after a relative long period (fiber may disappear when reaction process is over 4 h). Apparently, the detailed information associated with the phase compositions, types, structures and their forming mechanisms still need to be further explored [28].

The aim of this work is to precisely determine the newly formed phases and examine the tensile behavior of SMAFR laminated composites. Firstly, in order to determine the precise components of each phase via common methods (XRD, EDS and SEM etc.), a novel class of laminated materials was synthesized for the first time using Ti, Al and NiTi plates, in which there were sufficient amounts of reaction products and residual NiTi alloy after reaction. Then the new reacted phases were characterized. Secondly, the tensile behavior of SMAFR laminated composites at room temperature was investigated via quasi-static tensile tests, and the fracture mechanisms were investigated based on the SEM observation on fractured surface. Finally, the compression performance of the novel shape memory alloy NiTi plate-reinforced (SMAPR) Ti-Al laminated composites at room temperature was preliminarily studied via quasi-static compression tests.

2. Experimental procedures

2.1. Materials fabrication

SMAFR laminated composites was fabricated via vacuum hot pressing method using Ti alloy (Ti-6Al-4V) foils (100 mm × 100 mm × 0.55 mm), Al 1060 foils (100 mm × 100 mm × 0.6 mm) and NiTi fibers (Φ = 0.5 mm). It should be pointed out Ti alloy (Ti-6Al-4V) is used in this study in that it exhibits superior mechanical performance compared to that of commercial pure Ti, and Ti refers to Ti alloy (Ti-6Al-4V) throughout this paper. Given the uneven phases of the SMAFR laminated composites and the underlying possibility that the fiber may overreact after a relative long time, NiTi plates (have similar compositions, heat treatment and sintering process, etc. to the NiTi fiber) were purchased from the same company to fabricate shape memory alloy NiTi plate-reinforced (SMAPR) Ti-Al laminated composites. Based on this, the accurate components can be determined. The chemical compositions of the starting materials used in this work are shown in Table 1.

Similar to the preparation of SMAFR laminated composites, the plates for fabricating SMAPR laminated composites were also pretreated. Ti plates (100 mm × 100 mm × 0.55 mm), Al plates (100 mm × 100 mm × 0.9 mm) and NiTi plates (100 mm × 100 mm × 0.8 mm) were cut using the metal plate shearing machine, and then polished using silicon carbide paper to remove surface oxide layers, followed by alcohol bath via an ultrasonic cleaning machine for 15min. Thereafter, all the plates were rinsed using alcohol and then dried. All these procedures were well prepared for fabricating the SMAPR laminated composites.

The plates and fibers were stacked in an order "Ti-Al-NiTi-Al-Ti", which was defined as one unit. These units were placed in order, and the bottom and top layers of the stack were covered by TC4 plates, as is shown in Fig. 1. The fabrication process of SMAPR was almost identical to that of SMAFR laminated composites. Given that the NiTi plate would not be consumed so fast as NiTi fiber due to its large amount, the preservation period was prolonged to 5 h at the temperature of 660 °C for fabricating SMAPR laminated composites, whereas the preservation period was 2.5 h for fabricating SMAFR laminated composites. The loading pressure was set to 3 MPa for each stack except for the temperature preservation process at 660 °C. Detailed parameters of the fabrication process can be seen elsewhere [28].

2.2. Microstructure characterization

Phase constituent analysis of SMAPR laminated composites was conducted by X'Pert PRO X-ray diffraction (XRD) with the scan speed of 4°/min from 10° to 90°. The microstructure characterization of SMAPR laminated composites was performed by FEI Quanta 200 scanning electron microscopy (SEM, BSE mode) equipped with an EDS system. The fractured surface of SMAFR composites after tensile tests was observed by Hitachi SU-70 scanning electron microscopy (SEM, SE mode).

2.3. Mechanical testing

Tensile tests of SMAFR laminated composites were carried out on Instron 5500R load frame at the strain rate of 0.001/s under room temperature (23 °C). Three samples machined from the same SMAFR composites (volume fraction: 41%Ti, 2.5% NiTi) were tested under the condition of loading parallel to the fiber orientation, and the tensile tests of the Ti/Al_3Ti laminated composites with the same volume fraction of Ti but without NiTi were also conducted for comparison. During the tensile test, an extensometer was used to monitor the deformation of the sample. Moreover, NiTi fiber (Φ = 0.5 mm) subjected to the same heat treatment as SMAFR laminated composites was also observed by SEM-SE. In order to preliminarily exploit the potential application of the new SMAPR laminated composites (volume fraction: 21%Ti, 31% NiTi), compression tests were also conducted with load perpendicular to layers at the same strain rate and temperature. The stress-strain curves were plotted in the form of engineering stress and engineering strain data, and the same convention was used throughout

Table 1
Chemical compositions of TC4 plate, Al plate, NiTi plate and NiTi fiber.

Materials	Composition (wt%)
Ti-6Al-4V (TC4)	Ti: balance, Al:5.5–6.8, V:3.5–4.5, Fe = 0.30, C = 0.10, N = 0.05,H = 0.015, O = 0.20
Al 1060	Al: balance, Si:0.25, Cu:0.05, Zn:0.05, Mn:0.03, Mg:0.03, Fe:0.35, Ti:0.03, V:0.05
NiTi plate	Ti: balance, Ni: 55.89, C:0.045, N:0.003, O:0.043, H:0.002
NiTi fiber	Ti: balance, Ni:55.83, C:0.04, N:0.004–0.005, O:0.04, H:0.001, other elements<0.4

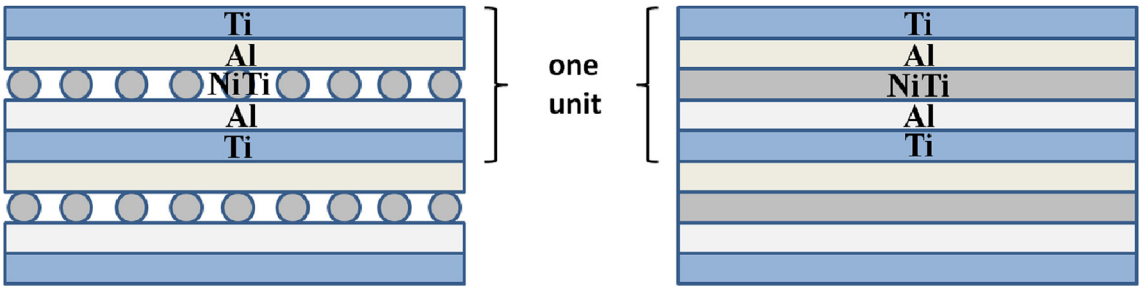

Fig. 1. Schematic diagrams of Ti plates, Al plates, NiTi fibers/plates used for fabricating SMAFR and SMAPR laminated composites.

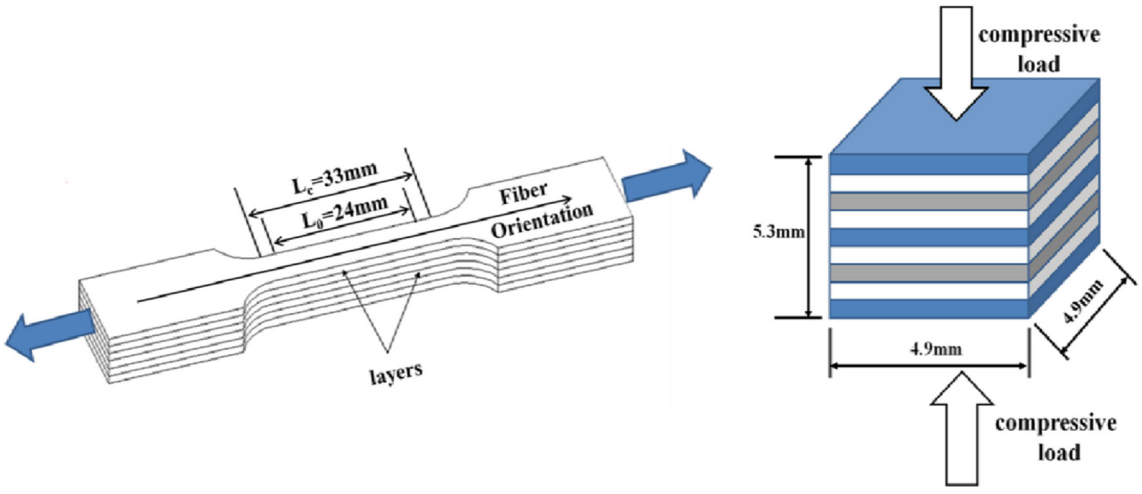

Fig. 2. Loading scheme and configuration of tensile specimen of SMAFR laminated composites and compressive specimen of SMAPR laminated composites.

this work. Detailed information of mechanical test samples can be found in Fig. 2.

3. Results and discussion

3.1. Microstructure characterization

In our recent work [28], some potentially formed products in SMAFR laminated composites, including Al_3Ti, Al_3Ni and $AlNi_2Ti$, are detected via XRD. SMAPR laminated composites consists of large amounts of new products, and it is a class of relatively uniform material compared with SMAFR laminated composites, such that the microstructure analysis is more convenient and convincing. As shown in Fig. 3, the XRD patterns reveal that Al_3Ti and Al_3Ni are the only intermetallic products formed in this fabrication process. It is worth noting that there are no Al-Ni-Ti ternary compounds formed during the fabrication process, while the residual Al is also observed.

Fig. 4 is a SEM-BSE image that shows microstructure of SMAPR laminated composites. It is noted that this new kind of laminated composites has a complicated microstructure, which consists of Ti layer, Al_3Ti layer, intermetallic layer and NiTi layer. The reaction band is clearly seen between NiTi layer and the intermetallic layer due to the diffusion reaction during the vacuum hot pressing process. Moreover, the mismatch of the thermal expansion coefficient of different phases gives rise to the occurrence of crack, as marked in Fig. 4. Such micro-cracks can be alleviated by adjusting the pressure, temperature and other parameters [28].

Fig. 5 shows the SEM-BSE images of NiTi layer and Ti layer with high magnification, and Fig. 6 shows the details of the intermetallic

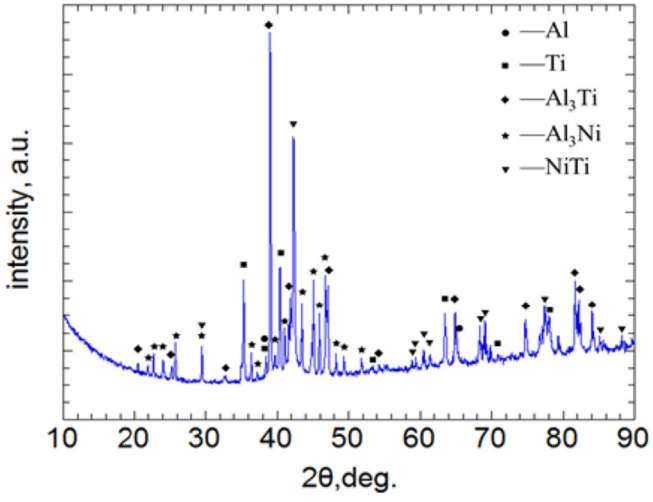

Fig. 3. XRD patterns of SMAPR laminated composites, showing that Al_3Ti and Al_3Ni formed during the fabrication process. In addition, residual Al is also observed besides Ti and NiTi.

layer. In order to determine the phases accurately, EDS analysis was performed in Areas A-F and spectrums 1–2, and the results are listed in Table 2. It can be seen in Fig. 5 (a) that the side near NiTi layer of the reaction band is relatively straight, whereas the side near the intermetallic layer exhibits jagged shape. No cracks are found along the interface for both sides, indicating that the bonding formed is superior as a result of metallurgical reaction. Close to the

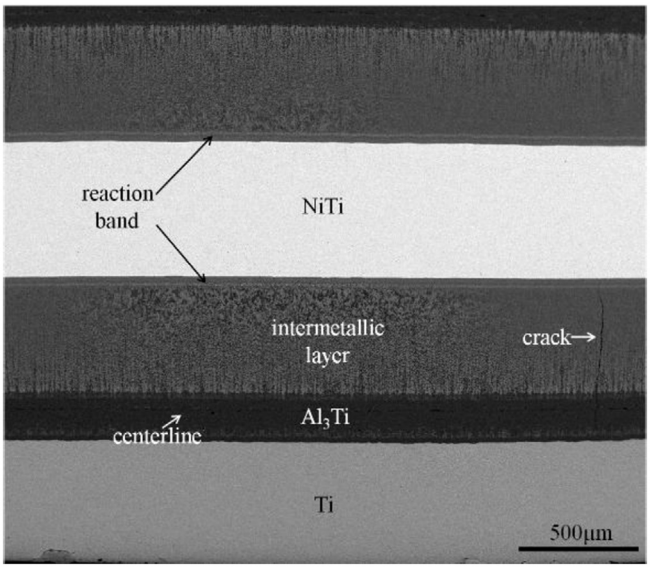

Fig. 4. SEM image of the microstructure of SMAPR laminated composites, including ductile Ti layer, Al_3Ti layer, intermetallic layer, NiTi layer and reaction band between intermetallic layer and NiTi layer.

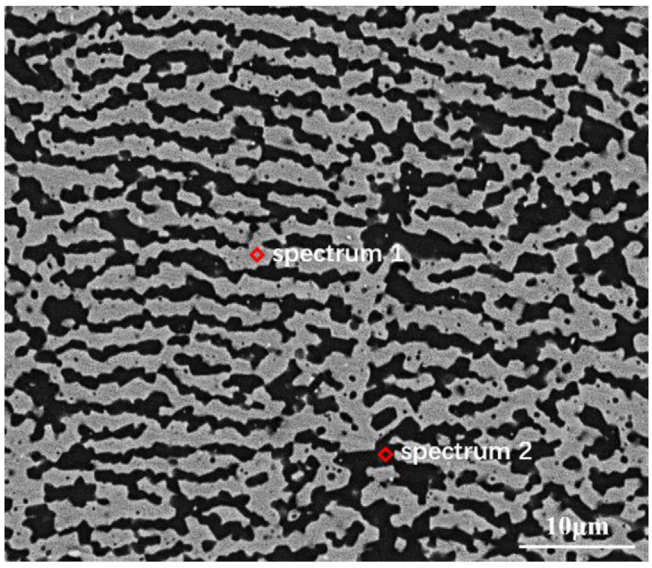

Fig. 6. SEM-BSE image of the intermetallic layer, showing two phases coexist in this layer. XRD and EDS analysis indicated the white phase is Al_3Ni, and the dark phase is Al_3Ti.

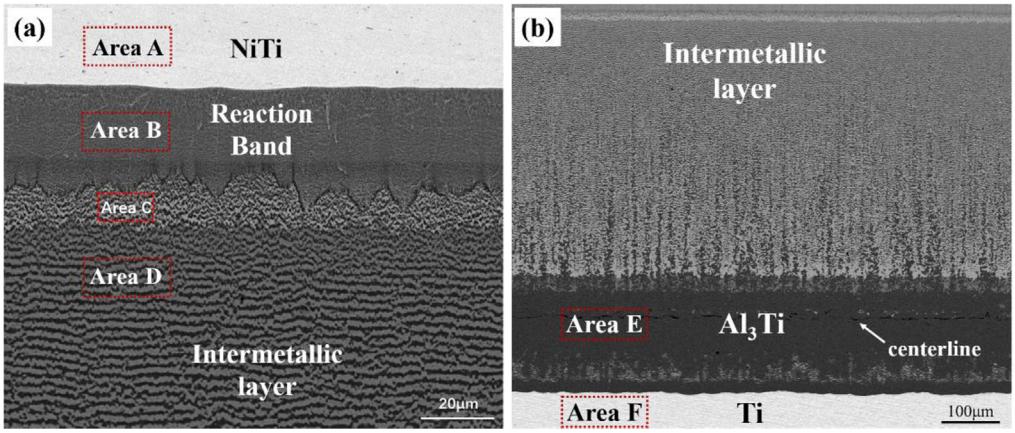

Fig. 5. SEM-BSE images near NiTi layer (a), showing the morphology of the side near the intermetallic layer of the reaction band exhibits jagged shape, and both Area B and Area C are transition layers to form Al_3Ni and Al_3Ti; and images near Ti layer (b), indicating Al_3Ti occurs near Ti layer, while some diffusion traces are also observed.

jagged-shape side of the reaction band, the phase components (Area C) appear to be distinct compared to those of the farther location (Area D). It is considered that the intermetallic layer marked as Area C, as well as the reaction band marked as Area B, constitutes the transition layer that contains two kinds of intermetallics, as can be seen in white and dark colors in the intermetallic layer in Fig. 5 (a). In Fig. 5 (b), Al_3Ti is found near Ti layer, and what's interesting is that a centerline is also observed, which was discussed in Harach's work [29] associated with Ti/Al_3Ti laminated composites. Some fasciculate traces are observed in the intermetallic layer close to Al_3Ti, indicating that the diffusion reaction was still in progress when the fabrication process was complete. Fig. 6 shows the SEM-BSE image of the intermetallic layer with high magnification. Combined the XRD (see Fig. 3) with EDS analysis (spectrums 1–2), it can be concluded that regardless of residual Al, the white phase is Al_3Ni, and the dark phase is Al_3Ti.

In order to analyze the diffusion reaction process, the atom ratios of Al/Ni, Ti/Ni and Ni/Ni in Areas A-D are plotted in Fig. 7. Here it is assumed that Ti atoms in Areas A-C are provided by NiTi layer, given the relatively long distance from Ti layer to the reaction band. It can be seen that the atom ratio of Ti-Ni in Area A is approximately equivalent to that of Ti-Ni in Area B. But in Area C, Ni atoms are more than Ti atoms, which means that Ni element can spread more easily than Ti provided by NiTi layer. In Area D, Ti is predominant compared with Ni, which may be the consequence of Ti element

Table 2
Typical chemical compositions of each layer and phase detected by EDS.

	Al		Ti		Ni		V	
	Wt%	At.%	Wt%	At.%	Wt%	At.%	Wt%	At.%
Area A	0	0	49.02	54.10	50.98	45.90	0	0
Area B	66.08	79.20	17.10	11.54	16.82	9.26	0	0
Area C	64.95	78.77	13.55	9.26	21.49	11.98	0	0
Area D	72.07	83.48	13.75	8.97	14.18	7.55	0	0
Area E	71.83	81.94	27.18	17.47	0	0	0.98	0.59
Area F	11.91	19.38	85.44	78.33	0	0	2.66	2.29
Spectrum 1	71.61	84.38	1.53	1.02	26.1	14.13	0.76	0.48
Spectrum 2	71.88	82.28	24.55	15.83	3.46	1.82	0.11	0.07

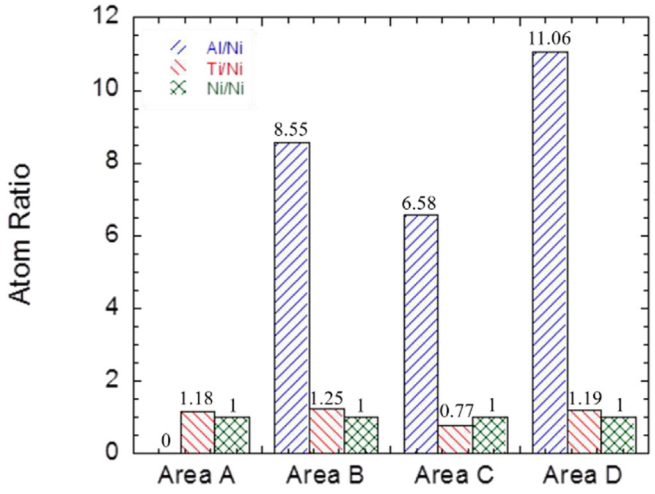

Fig. 7. Atom ratios of Al/Ni, Ti/Ni and Ni/Ni in Areas A-D, showing the element distribution in each area.

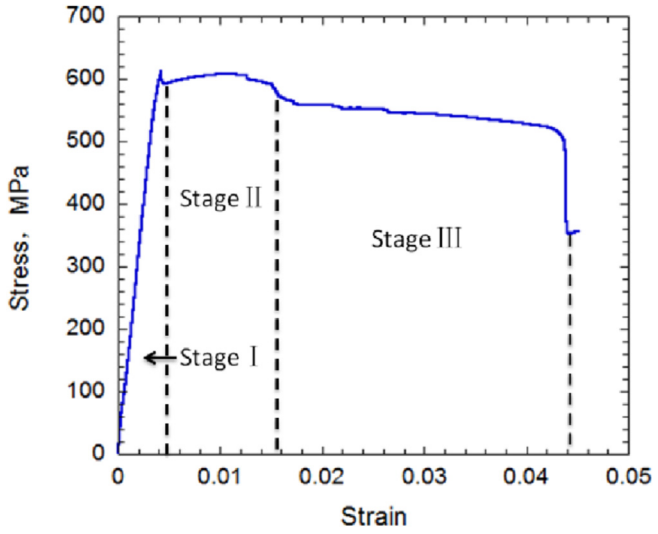

Fig. 8. Typical stress-strain curve of SMAFR laminated composites, showing a three-stage behavior, which includes the delamination of the interface between Ti and Al_3Ti, the fracture of intermetallic phase and the fracture of Ti as well as NiTi fiber.

offered by Ti (Al_3Ti) layer diffusing to Area D. In terms of Al, it is clearly seen that most of Al atoms are enriched in Area D, where Al plate was placed originally. In Area C, the atom ratio between Al and Ti + Ni is approximately equal to 3:1, which means in this area, the main phases are Al_3Ti and Al_3Ni. During the diffusion reaction, some Al atoms are enriched in Area B (reaction band), rendering Al atoms more than that in Area C, but they cannot break the barrier formed by NiTi/reaction band interface, which is proved from the fact that no Al atoms can be detected by EDS in Area A.

It can be found that the microstructure of SMAPR laminated composites is of overwhelming complication. After vacuum hot pressing process, the original "Ti-Al-NiTi-Al-Ti" unit has been replaced by "Ti-Al_3Ti-intermetallic layer (Al_3Ti + Al_3Ni)-reaction band-NiTi-reaction band-intermetallic layer-Al_3Ti-Ti" as a new unit, which presents a typical multilayer structure. According to the XRD and EDS analysis results, each phase of SMAPR laminated composites is determined. The most significant finding is that the intermetallic layer is composed of Al_3Ti phase and Al_3Ni phase, along with residual Al; no other intermetallics are found in the intermetallic layer. It should be pointed out that in the Al_3Ti layer near Ti layer, there exists the phase of $Al_3Ti_{0.8}V_{0.2}$. The XRD patterns of $Al_3Ti_{0.8}V_{0.2}$ are almost identical to those of Al_3Ti, and considering the small amount of V, $Al_3Ti_{0.8}V_{0.2}$ is neglected in this section. In addition, the thickness consumption of NiTi layer and Ti layer differs a lot. Take the NiTi layer and Ti layer in the interior of the laminated composites as an example, the original thickness of NiTi is 800 μm, whereas the thickness of original Ti is 550 μm. After the fabrication process, the thicknesses of NiTi and Ti are determined to be 661.8 μm and 506.7 μm, respectively. The reduction of NiTi thickness, 138.2 μm, is triple that of Ti thickness, 43.3 μm, indicating that the consumption of NiTi is far more drastic compared with Ti layer during this fabrication process, which is exceedingly important to have the laminated composites tailored according to the engineering applications. Future work will focus on the diffusion process in this laminated structure.

3.2. Tensile behavior of SMAFR laminated composites

Fig. 8 shows the typical tensile stress-strain curve of SMAFR laminated composites. The curve shows a three-stage behavior. Stage I mainly includes the elastic stage of this curve, along with the yield stage. At the end of Stage I, it can be seen that a sudden drop occurs due to the delamination of interface between Ti and Al_3Ti. After that, the Ti layer, intermetallic layer and NiTi fiber suffer from the tensile load. Stage II ends up with the fracture of intermetallic layer. Stage III exhibits obvious plastic deformation as the ductile Ti and NiTi fiber bear the load and they contribute the ductility to stress-stain behavior. The ultimate tensile stress (UTS) and failure strain of each sample of SMAFR laminated composites, as well as Ti/Al_3Ti laminated composites are listed in Table 3 for comparison. It can be seen that the average UTS of SMAFR laminated composites is 613 MPa, and the average failure strain is 4.6%, both of which are greater than those of Ti/Al_3Ti laminated composites. The improvement of tensile performance is attributed to the reinforcement of NiTi fiber and the new intermetallic layer, which will be discussed in the next section of this paper.

3.3. Fracture mechanisms of SMAFR laminated composites

The tested samples of SMAFR laminated composites failed into two parts after quasi-static tensile tests. In order to reveal the fracture mechanisms of SMAFR laminated composites, all fractured surfaces of the tested samples were observed via Hitachi SU-70 scanning electron microscope (SEM) in SE mode. The typical fracture characteristics observed from the overall fractured sample surface, fractured Ti layer, intermetallic layer, and NiTi fiber are shown in Fig. 9. It can be seen in Fig. 9 (a) that the delamination occurs between Ti layer and Al_3Ti layer, and the pulling-out of NiTi fibers can be conspicuously observed. It is remarkably significant to find that the intermetallic phase around the fiber comes into being a "block". Unlike the Ti/Al_3Ti laminated composites, whose Al_3Ti

Table 3
The UTS and fracture strain of SMAFR laminated composites and Ti/Al_3Ti.

Material	Number	UTS, MPa	Failure strain
SMAPR laminated composites	1	612.5	4.4%
	2	607.3	4.9%
	3	620.2	4.5%
	Average	613.3	4.6%
Ti/Al_3Ti laminated composites	1	436.4	4.2%
	2	453.3	4.3%
	3	433.7	4.0%
	Average	441.1	4.2%

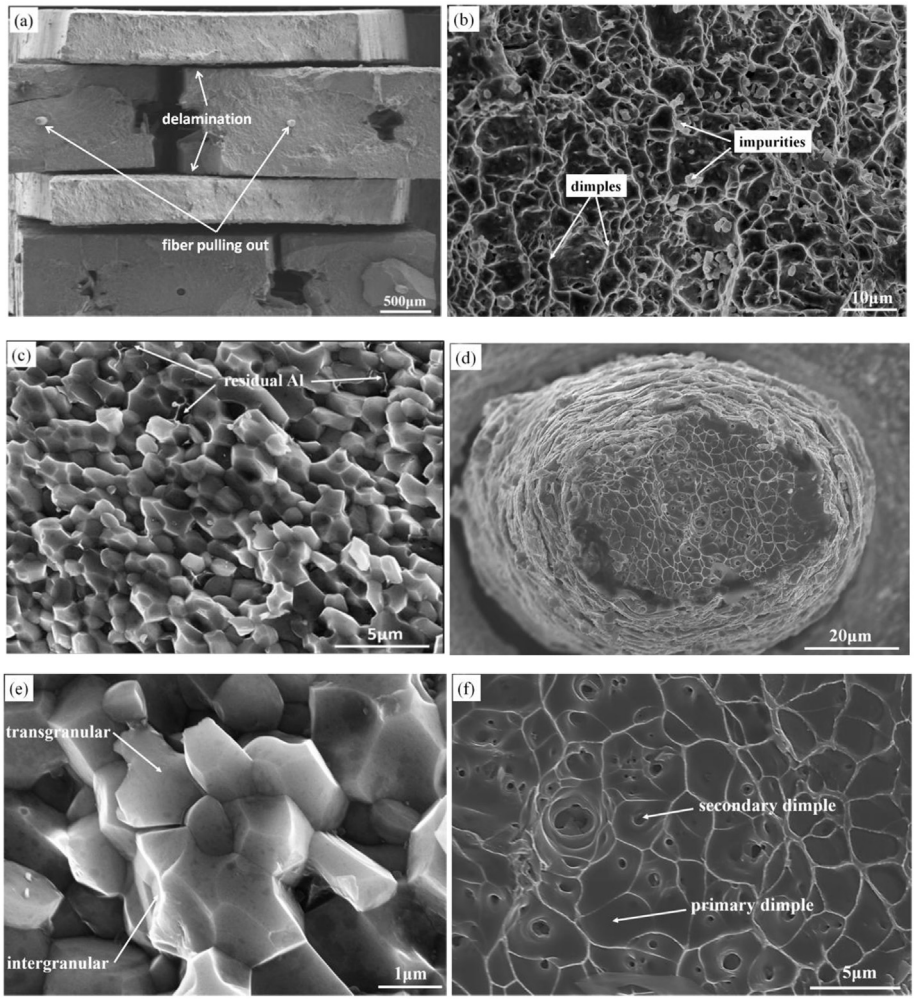

Fig. 9. SEM images of the typical fracture characteristics observed from the overall fractured sample surface (a), fractured Ti layer (b), intermetallic layer (c), and NiTi fiber (d); high magnification SEM image of Al_3Ti (e), and high magnification SEM image of the interior of NiTi in SMAFR laminated composites(f).

layer breaks into small pieces after tension, leading to the difficulty in fracture mechanism analysis via SEM observation, the intermetallic phases in SMAFR laminated composites form into blocks after the tensile testing, which contributes to the superior tensile performance of this novel kind of fiber reinforced laminated structure. Fig. 9 (b) shows the fracture surface features of Ti. It can be seen that the surface of fractured Ti has numerous dimples, and exhibits obvious plastic deformation, which plays an important role in the tensile behavior of SMAFR laminated composites. As seen in Fig. 9 (c) and (e), the fracture of intermtallic layer presents typical brittle fracture, and some residual Al as marked can be found in some regions. The major fracture mode observed is intergranular fracture. Transgranular fracture is also found in this layer, but it only takes a relatively small portion compared to the intergranular fracture surface. In terms of Al_3Ti layer, the fracture mode is almost identical to the mixed intermetallic layer, so it won't be discussed here repeatedly. It can be seen in Fig. 9 (d) and (f), necking phenomenon occurs on NiTi fiber with a reaction band around it, and a clear gap between the fiber and intermetallic matrix can be observed. In addition, primary dimples and secondary dimples are found in the interior of the fiber due to the superior ductility of superelastic NiTi alloy, which is consistent with some other researches [30–32].

In order to testify the effect of NiTi fiber, another quasi-static tensile test using NiTi fiber experienced the same heat treatment as the SMAFR laminated composites was carried out and the fracture was observed via SEM, as is shown in Fig. 10 (a). It can be seen in Fig. 10 (a) that the necking phenomenon occurs, and a shear lip is also found in the fracture surface of NiTi fiber. Similar to the NiTi fiber in SMAFR laminated composites as reinforcement, a multitude of dimples are observed in the interior of the fiber, which prove that the NiTi fiber still holds its ductility to some extent after the hot pressing process. Fig. 10 (b) shows the gap between the fiber and the intermetallic layer. It can be seen that the reaction band is of jagged shape, which conforms to the microstructure of reaction band as aforementioned. Otherwise, such a unique shape of bonding (reaction band) between fiber and matrix can transform the load to fiber reinforcement from matrix and contributes a lot to the tensile performance of the SMAFR laminated composites. In brief, the tensile properties of SMAFR laminated composites are closely related to each component. All the components, including Ti layer, intermetallic layer, NiTi fiber, as well as the reaction band, provide their contributions to the overall superior tensile performance of SMAFR laminated composites.

3.4. Compressive response of SMAPR laminated composites

In order to preliminarily exploit the potential application of the

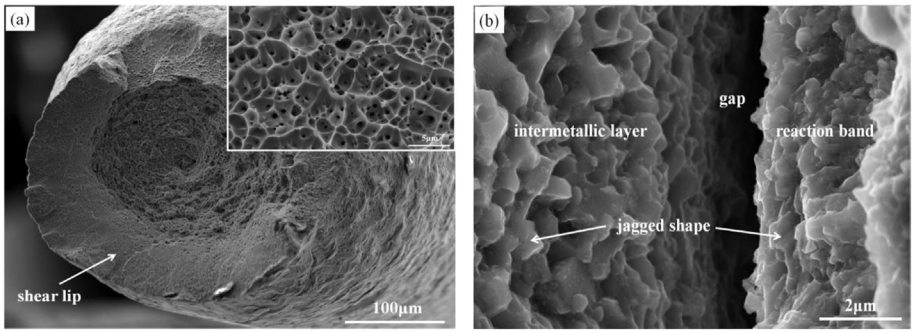

Fig. 10. SEM images of fiber experienced the same heat treatment as SMAFR laminated composites (a), and the gap between the fiber and intermetallic layer in SMAFR laminated composites after tension (b), showing jagged shape on both sides.

new SMAPR laminated composites (volume fraction: 21%Ti, 31% NiTi), mechanical response is essential to study under compressive stress state. The compression tests were conducted using 5 samples with loading perpendicular to layers at the strain rate of 0.001/s. The stress-strain curves and the results of the compression tests are shown in Fig. 11 and Table 4, respectively. The experimental results showed that the average peak compressive strength of SMAPR laminated composites is 1105 MPa, slightly lower than that of SMAFR laminated composites [25] due to the larger volume fraction of ductile layer, Ti layer and NiTi layer. However, the average failure strain increases to 5.1%. It is noted that fluctuation occurs on stress-strain curves after the linear stage, which mainly because the ductile layer, including Ti and superelastic NiTi alloy, may not fracture when the intermetallic layer breaks, unlike the Ti/Al_3Ti laminated composites, showing a diagonal shear failure [5]. The preliminary mechanical tests indicated that this novel kind of laminated composites possesses excellent mechanical properties, which prove it is a promising candidate in engineering applications.

4. Conclusions

In the present study, a novel kind of shape memory alloy NiTi plate reinforced (SMAPR) laminate composites was successfully fabricated via vacuum hot pressing process to help accurately determine the detailed phases of the shape memory alloy NiTi fiber reinforced (SMAFR) laminate composites. Otherwise, the tensile behavior of SMAFR laminated composites and compressive properties of SMAPR laminated composites were also investigated. The main conclusions drawn from the current work are summarized as follows:

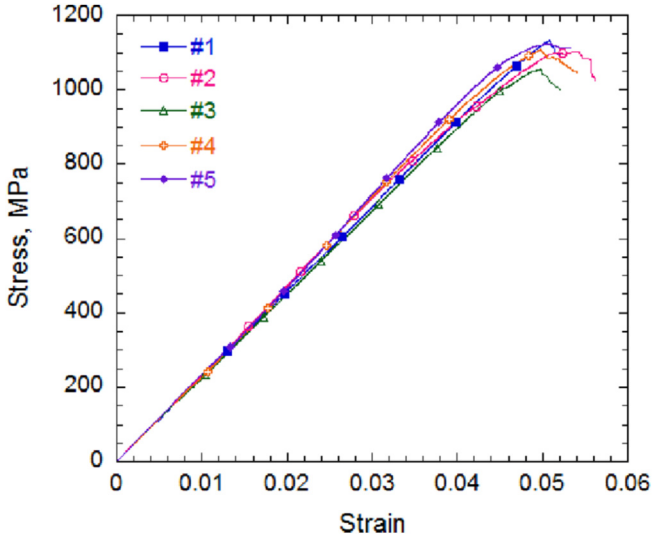

Fig. 11. The compression stress-strain curves of the samples tested with the loading perpendicular to the layers at the strain rate of 0.001/s.

Table 4
The compressive strength and failure strain of SMAPR laminated composites under quasi-static compression.

Number	Compressive Strength, MPa	Failure strain
1	1133.9	5.1%
2	1105.5	5.4%
3	1055.6	4.9%
4	1112.5	4.9%
5	1119.5	5.0%
Average	1105.4	5.1%

(1) The microstructure of SMAPR laminated composites is of overwhelming complication. After vacuum hot pressing process, the original "Ti-Al-NiTi-Al-Ti" unit was replaced by "Ti-Al_3Ti-intermetallic layer (Al_3Ti + Al_3Ni)-reaction band-NiTi-reaction band-intermetallic layer-Al_3Ti-Ti" as a new unit, which presents a typical multilayer structure. XRD and EDS analysis showed that the intermetallic layer of SMAPR laminated composites is composed of Al_3Ti phase and Al_3Ni phase, along with residual Al, and no other intermetallics is found in the intermetallic layer.

(2) The quasi-static tensile tests indicated that the tensile performance of SMAFR laminated composites is superior to that of Ti/Al_3Ti composites. The fracture process contains three basic stages: (I) delamination of interface of Ti/Al_3Ti, (II) fracture of intermetallic layer, and (III) fracture of Ti layer and NiTi fiber. The average ultimate tensile strength (UTS) is 613 MPa, and the average failure strain is 4.6%, both of which are greater than that of Ti/Al_3Ti laminated composites.

(3) The tensile fracture of SMAFR laminated composites was observed via SEM observation, and the fracture mechanisms are determined. Ti layer and NiTi fiber exhibits typical ductile fracture, whereas the intermetallic layer shows brittle fracture, in which the major fracture is intergranular, along with minor transgranular fracture mode. Moreover, SEM observation demonstrated that NiTi fiber in SMAFR laminated composites still holds ductility to some extent, which can improve the tensile performance of the laminated structure.

(4) The preliminary compressive tests of SMAPR laminated composites indicated that the average compressive strength is 1105 MPa, and the average strain to failure is 5.1%. Due to the ductility of Ti, and especially the superelastic NiTi alloy,

the overall compressive performance is enhanced. In all, this kind of materials possesses good mechanical properties and opens a brand new perspective in the realm of the laminated structure.

Acknowledgements

The authors gratefully acknowledge the financial supports of this study by the National Natural Science Foundation of China (No 51671065), Key Program of Natural Science Foundation of Heilongjiang Province (ZD2015012), Shanghai Aerospace Science and Technology Innovation Fund Project (SAST2016052), and the Fundamental Research Funds for the Central Universities of Harbin Engineering University (No. GK2100260155).

References

[1] D.J. Harach, K.S. Vecchio, Microstructure evolution in metal-intermetallic laminate (MIL) composites synthesized by reactive foil sintering in air, Metall. Mater. Trans. A-Phys. Metall. Mater. Sci. 32 (6) (2001) 1493–1505.
[2] J. Hu, Q. Zhang, Y. Liu, et al., Phase transformation behaviors of TiNi fibers embedded in an aluminum matrix, J. Alloys Compd. 589 (2014) 491–497.
[3] R.R. Adharapurapu, K.S. Vecchio, F. Jiang, et al., Effects of ductile laminate thickness, volume fraction, and orientation on fatigue-crack propagation in Ti-Al_3Ti metal-intermetallic laminate composites, Metall. Mater. Trans. A-Phys. Metall. Mater. Sci. 36 (6) (2005) 1595–1608.
[4] J. Oh, W. Lee, S.G. Pyo, W. Park, S. Lee, N.J. Kim, Microstructural analysis of multilayered titanium aluminide sheets fabricated by hot rolling and heat treatment, Metall. Mater. Trans. A-Phys. Metall. Mater 33 (12) (2002) 3649–3659.
[5] R.D. Price, F. Jiang, R.M. Kulin, K.S. Vecchio, Effects of ductile phase volume fraction on the mechanical properties of Ti–Al3Ti metal-intermetallic laminate (MIL) composites, Mater. Sci. Eng. A-Struct. Mater. Prop. Microstruct. Process 528 (7) (2011) 3134–3146.
[6] D.V. Lazurenko, V.I. Mali, I.A. Bataev, et al., Metal-intermetallic laminate Ti-Al_3Ti composites produced by spark plasma sintering of titanium and aluminum foils enclosed in titanium shells, Metall. Mater. Trans. A 46 (9) (2015) 4326–4334.
[7] K.S. Vecchio, Synthetic multifunctional metallic-intermetallic laminate composites, JOM 57 (3) (2005) 25–31.
[8] D.J. Harach, Processing, Properties, and Ballistic Performance of Titanium-aluminum Titanium Metal-intermetallic Laminate (MIL) Composites, 2000.
[9] T. Li, F. Grignon, D.J. Benson, et al., Modeling the elastic properties and damage evolution in Ti–Al 3 Ti metal–intermetallic laminate (MIL) composites, Mater. Sci. Eng. A 374 (1) (2004) 10–26.
[10] T. Li, F. Jiang, E.A. Olevsky, et al., Damage evolution in Ti6Al4V–Al_3Ti metal-intermetallic laminate composites, Mater. Sci. Eng. A 443 (1) (2007) 1–15.
[11] Y. Cao, C. Guo, S. Zhu, et al., Fracture behavior of Ti/Al 3 Ti metal-intermetallic laminate (MIL) composite under dynamic loading, Mater. Sci. Eng. A 637 (2015) 235–242.
[12] F. Jiang, R.M. Kulin, K.S. Vecchio, Use of Brazilian disk test to determine properties of metallic-intermetallic laminate composites, JOM 62 (1) (2010) 35–40.
[13] P. Zhou, C. Guo, E. Wang, et al., Interface tensile and fracture behavior of the Ti/Al_3Ti Metal-Intermetallic Laminate (MIL) composite under quasi-static and high strain rates, Mater. Sci. Eng. A 665 (2016) 66–75.
[14] A. Rohatgi, D.J. Harach, K.S. Vecchio, et al., Resistance-curve and fracture behavior of Ti–Al_3Ti metallic–intermetallic laminate (MIL) composites, Acta Mater. 51 (10) (2003) 2933–2957.
[15] U.R. Kattner, J C,Lin Y A Chang. Thermodynamic assessment and calculation of the Ti-Al system, Metall. Mater. Trans. A 23 (8) (1992) 2081–2090.
[16] J.L. Murray, Phase diagrams of binary titanium alloys, ASM Int. (1987) 354.
[17] Y. Mishin, C. Herzig, Diffusion in the Ti–Al system, Acta Mater. 48 (3) (2000) 589–623.
[18] T.L. Turner, C.L. Lach, R.J. Cano, in: SPIE 8th Annual Inter. Symp. On Smart Struct. and Mater. Active Materials:Behavior and Mech, vol. 4333, SPIE, Newport Beach, March 4-8, 2001. Paper No.4333–60.
[19] W. Guo, H. Kato, Submicron-porous NiTi and NiTiNb shape memory alloys with high damping capacity fabricated by a new top-down process, Mater. Des. 78 (2015) 74–79.
[20] G. Song, N. Ma, H.N. Li, Applications of shape memory alloys in civil structures, Eng. Struct. 28 (9) (2006) 1266–1274.
[21] E.J. Graesser, F.A. Cozzarelli, Shape-memory alloys as new materials for aseismic isolation, J. Eng. Mech. 117 (11) (1991) 2590–2608.
[22] S.M. Saghaian, H.E. Karaca, M. Souri, et al., Tensile shape memory behavior of $Ni_{50.3}$ $Ti_{29.7}Hf_{20}$ high temperature shape memory alloys, Mater. Des. 101 (2016) 340–345.
[23] J. Raghavan, T. Bartkiewicz, S. Boyko, et al., Damping, tensile, and impact properties of superelastic shape memory alloy (SMA) fiber-reinforced polymer composites, Compos. Part B Eng. 41 (3) (2010) 214–222.
[24] D.J. Hartl, D.C. Lagoudas, Aerospace applications of shape memory alloys, Proc. Inst. Mech. Eng. Part G J. Aero. Eng. 221 (4) (2007) 535–552.
[25] M. Samadpour, H. Asadi, Q. Wang, Nonlinear aero-thermal flutter postponement of supersonic laminated composite beams with shape memory alloys, Eur. J. Mech-A/Solids 57 (2016) 18–28.
[26] A. Treviso, B.V. Genechten, D. Mundo, et al., Damping in composite materials: properties and models, Compos. Part B 78 (2015) 144–152.
[27] M.K. Kim, D.J. Kim, Y.S. Chung, et al., Direct tensile behavior of shape-memory-alloy fiber-reinforced cement composites, Const. Build. Mater. 102 (2016) 462–470.
[28] E. Wang, C. Guo, P. Zhou, et al., Fabrication, mechanical properties and damping capacity of shape memory alloy NiTi fiber-reinforced metal–intermetallic–laminate (SMAFR-MIL) composite, Mater. Des. 95 (2016) 446–454.
[29] D.J. Harach, K.S. Vecchio, Microstructure evolution in metal-intermetallic laminate (MIL) composites synthesized by reactive foil sintering in air, Metall. Mater. Trans. A 32 (6) (2001) 1493–1505.
[30] K. Yokoyama, K. Hamada, K. Moriyama, et al., Degradation and fracture of Ni–Ti superelastic wire in an oral cavity, Biomater. 22 (16) (2001) 2257–2262.
[31] R. Matsui, H. Tobushi, Y. Furuichi, et al., Tensile deformation and rotating-bending fatigue properties of a highelastic thin wire, a superelastic thin wire, and a superelastic thin tube of NiTi alloys, J. Eng. Mater. Technol. 126 (4) (2004) 384–391.
[32] G.N. Dayananda, M.S. Rao, Effect of strain rate on properties of superelastic NiTi thin wires, Mater. Sci. Eng. A 486 (1) (2008) 96–103.